EUROPEAN SOCIETY OF RADIOLOGY
Insights into Imaging

ORIGINAL ARTICLE

Open Access

Determining rib fracture age from CT scans with a radiomics-based combined model: a multicenter retrospective study

Yilin Tang[1†], Liang Jin[1,2*†], Wenbin Ji[3], Zhuangxuan Ma[1], Dechun Li[1], Wei Hong[4*] and Ming Li[1,5*]

Abstract

Objectives We aimed to develop a combined model based on clinical and radiomic features to classify fracture age.

Methods We included 1219 rib fractures from 239 patients from our center between March 2016 and September 2022. We created an external dataset using 120 rib fractures from 32 patients from another center between October 2019 and August 2023. According to tasks (fracture age between < 3 and ≥ 3 weeks, 3–12, and > 12 weeks), the internal dataset was randomly divided into training and internal test sets. A radiomic model was built using radiomic features. A combined model was constructed using clinical features and radiomic signatures by multivariate logistic regression, visualized as a nomogram. Internal and external test sets were used to validate model performance.

Results For classifying fracture age between < 3 and ≥ 3 weeks, the combined model had higher areas under the curve (AUCs) than the radiomic model in the training set (0.915 vs 0.900, $p = 0.009$), internal test (0.897 vs 0.854, $p < 0.001$), and external test sets (0.881 vs 0.811, $p = 0.003$). For classifying fracture age between 3–12 and > 12 weeks, the combined model had higher AUCs than the radiomic model in the training model (0.848 vs 0.837, $p = 0.12$) and internal test sets (0.818 vs 0.793, $p < 0.003$). In the external test set, the AUC of the nomogram-assisted radiologist was 0.966.

Conclusion The combined radiomic and clinical model showed good performance and has the potential to assist in the classification of rib fracture age. This will be beneficial for clinical practice and forensic decision-making.

Critical relevance statement This study describes the development of a combined radiomic and clinical model with good performance in the classification of the age of rib fractures, with potential clinical and forensic applications.

Key points

• Complex factors make it difficult to determine the age of a fracture.

• Our model based on radiomic features performed well in classifying fracture age.

• Associating the radiomic features with clinical features improved the model's performance.

Keywords Radiomics, Rib fracture, Computed tomography, Machine learning

---

†Yilin Tang and Liang Jin contributed equally to this work.

*Correspondence:
Liang Jin
jin_liang@fudan.edu.cn
Wei Hong
Drivyh@126.com
Ming Li
ming_li@fudan.edu.cn
Full list of author information is available at the end of the article

Springer Open

Tang *et al. Insights into Imaging*   (2023) 14:214

Page 2 of 13

Graphical Abstract

Determining rib fracture age from CT scans with a radiomics-based combined model: a multicenter retrospective study
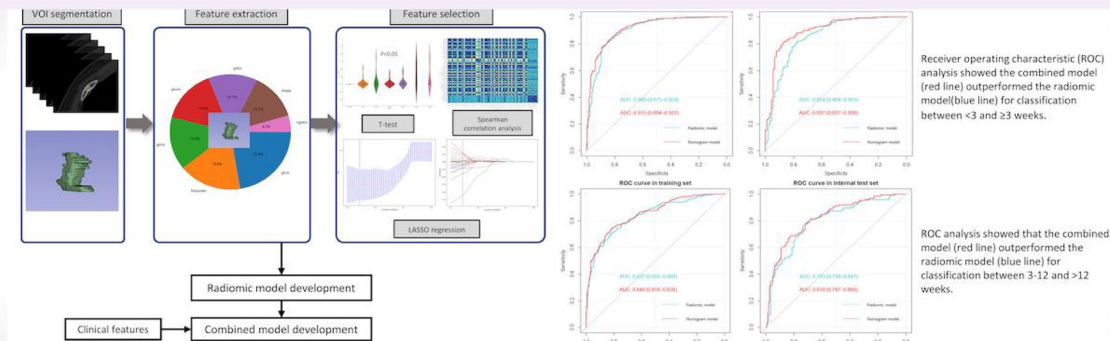
This study describes the development of a combined radiomic and clinical model with good performance in classification of the age of rib fractures, with potential clinical and forensic applications.

Insights Imaging (2023) Tang Y, Jin L, Ji W et al. DOI: 10.1186/s13244-023-01546-y

Introduction

Thoracic injuries are common among trauma patients [1]. Rib fractures are the most common form of thoracic trauma, serving as a marker of injury severity and a guide for legal decision-making [2, 3]. In the USA, 300,000 patients were diagnosed with rib fractures in 2004 [4], which increased to 350,000 in 2017 [5]. The risk of fracture increases significantly with age [6, 7]. Therefore, rib fracture cases are expected to increase with global aging [8]. The cause of rib fractures varies between age groups; they are usually caused by falls in older adults, traffic accidents in adults, and violent conflicts in adolescents [9, 10].

Accident compensation usually requires clarification of injury events leading to rib fractures [11]. In addition, the specific timing of rib fractures during accidents is important in legal cases. Providing the age of a rib fracture can clarify the association with a specific physical event and rule out irrelevant injuries, which is beneficial for settling compensation issues. Furthermore, the fracture healing state can be clinically assessed based on a patient's radiological presentation and physical examination at different ages after the fracture [12]. However, this is influenced by multiple factors, including the patient's age, nutritional status, sex, fracture location, and vascular injury, making it highly challenging to assess fracture union [13]. Combining imaging with fracture timing can improve surgeons' confidence in assessing the healing state. Analyzing the fracture healing process can guide further treatment and care practices for patients with rib fractures [14].

Radiomics provides a new perspective for doctors by extracting quantitative features from medical images to reflect the heterogeneity of lesions that are unobservable by the naked eye. Its primary benefit lies in the quantitative and more objective interpretation of medical images, potentially overcoming the limitations of visual image assessment [15, 16]. To the best of our knowledge, no study has investigated whether a model derived from computed tomography (CT) imaging and clinical information can aid the diagnosis of fracture age. We aimed to evaluate the performance of a model built using radiomic and clinical data to diagnose fracture age.

Methods

Ethics consideration

This retrospective study was approved by the ethics committee of our hospital (No. 20220069), which waived the requirement for informed consent.

Study population of the internal dataset

We searched the Picture Archiving and Communication System of our hospital using the keyword phrase "chest trauma evaluation" to identify patients who visited our hospital for chest trauma evaluation between March 2016 and September 2022. The inclusion criteria comprised the following: (1) patient age > 18 years; (2) patients who experienced a traumatic event (including traffic accidents, falls, and fights involving blunt chest trauma); (3) imaging reports confirming at least one rib fracture; (4) slice thickness after image reconstruction < 1.5 mm; and (5) case reports documenting the precise time of fractures. The exclusion criteria comprised the following: (1) malignant and benign bone tumors involving the ribs; (2) metastatic diseases involving the ribs; (3) significant artifacts in CT images; and (4) surgical internal fixation of rib fractures. We obtained demographic features, including age and sex, from the patient hospital records. The scan parameters are described in the Supplementary Material. We identified 71 patients with rib fractures imaged < 3 weeks after trauma and matched them by age to ensure that the number of fractures at 3–12 weeks and > 12 weeks was approximately equal to that at < 3 weeks. These three frames for depicting fracture ages were sourced from previously published literature [17, 18]. For each patient, 12 bilateral ribs were included in the dataset.

Finally, as shown in Fig. 1, based on our inclusion and exclusion criteria, 1219 rib fractures (< 3 weeks: $n = 323$; 3–12 weeks: $n = 492$; > 12 weeks: $n = 404$) from 239 patients (< 3 weeks: $n = 71$; 3–12 weeks: $n = 90$; > 12 weeks: $n = 78$) were included in our internal dataset. For classifying fracture age between < 3 and ≥ 3 weeks, 1219 fractures were randomly assigned to the training ($n = 853$) and internal test sets ($n = 366$). For classifying fracture age between 3–12 and > 12 weeks, 896 fractures were randomly assigned to the training ($n = 627$) and internal test sets ($n = 269$).

Study population of the external dataset

To build a validation external dataset, we included 120 rib fractures from 32 patients (< 3 weeks: $n = 16$; ≥ 3 weeks: $n = 16$) who underwent chest trauma evaluation between October 2019 and August 2023, in another hospital in Shanghai according to the same inclusion and exclusion criteria to construct. This external dataset was used to confirm the efficacy of our model and assess the performance of radiologists in classifying rib fracture age based on CT images using the model. The scan parameters used for CT examination are provided in the Supplementary Material. Detailed clinical features are listed in Table S3.

Extraction of radiomic and clinical features

Referring to the diagnostic CT reports, a radiologist with 5 years of experience in chest diagnostics manually delineated the volume of interest (VOI) at the fractured ends of the rib using the 3D Slicer software (https://www.slicer.org) (Figure S1). Subsequently, another radiologist with 20 years of experience in chest diagnostics confirmed the VOIs. Next, we used the PyRadiomics package in Python to extract radiomic features from the VOIs [19]. For each VOI, we extracted 107 radiomic features. The detailed outlining process and radiomic features are shown in the Supplementary Material.

The clinical features included demographic and CT image features. The clinical features were as follows: (1) pleural inflammation, (2) 1–4 rib fractures, (3) lateral fractures, (4) bone fragments, (5) multiple fractures of the same rib, (6) cartilage junction fractures, (7) periosteal callus information, (8) intramedullary callus information, and (9) sex.

Selection of radiomic and clinical features

We hypothesized that meaningful features might differ when classifying fracture age between < 3 weeks, ≥ 3 weeks, 3–12 weeks, and > 12 weeks. Therefore, we selected the features separately according to these time frames.

All radiomic features were normalized using *z*-score normalization before feature selection. To minimize the impact of dimensionality, the selection of features was conducted in three steps using the training set. First, we calculated the *p* value for each feature using the *t*-test and selected features with *p* values < 0.05 for further consideration. Spearman's correlation coefficients were calculated for the selected features to avoid the underlying severe linear dependence. When the value was < 0.9, we determined this to mean that there was no correlation between the selected features. Lastly, we used the least absolute shrinkage and selection operator (LASSO) analysis to determine the most useful radiomic features. Clinical features were selected using univariate and multivariate logistic regression analyses.

Development of radiomic and combined models

We used two feature sets instead of one for the precise classification of the fracture age because of the difference in features for fracture age between < 3 weeks, ≥ 3 weeks, 3–12 weeks, and > 12 weeks. Regarding both levels of classification, we developed radiomic and combined models.

The base classifier acts as a feature encoder and has a significant impact on classification [20]. We compared the performance of five common machine learning (ML)

Tang *et al. Insights into Imaging* (2023) 14:214

Page 4 of 13
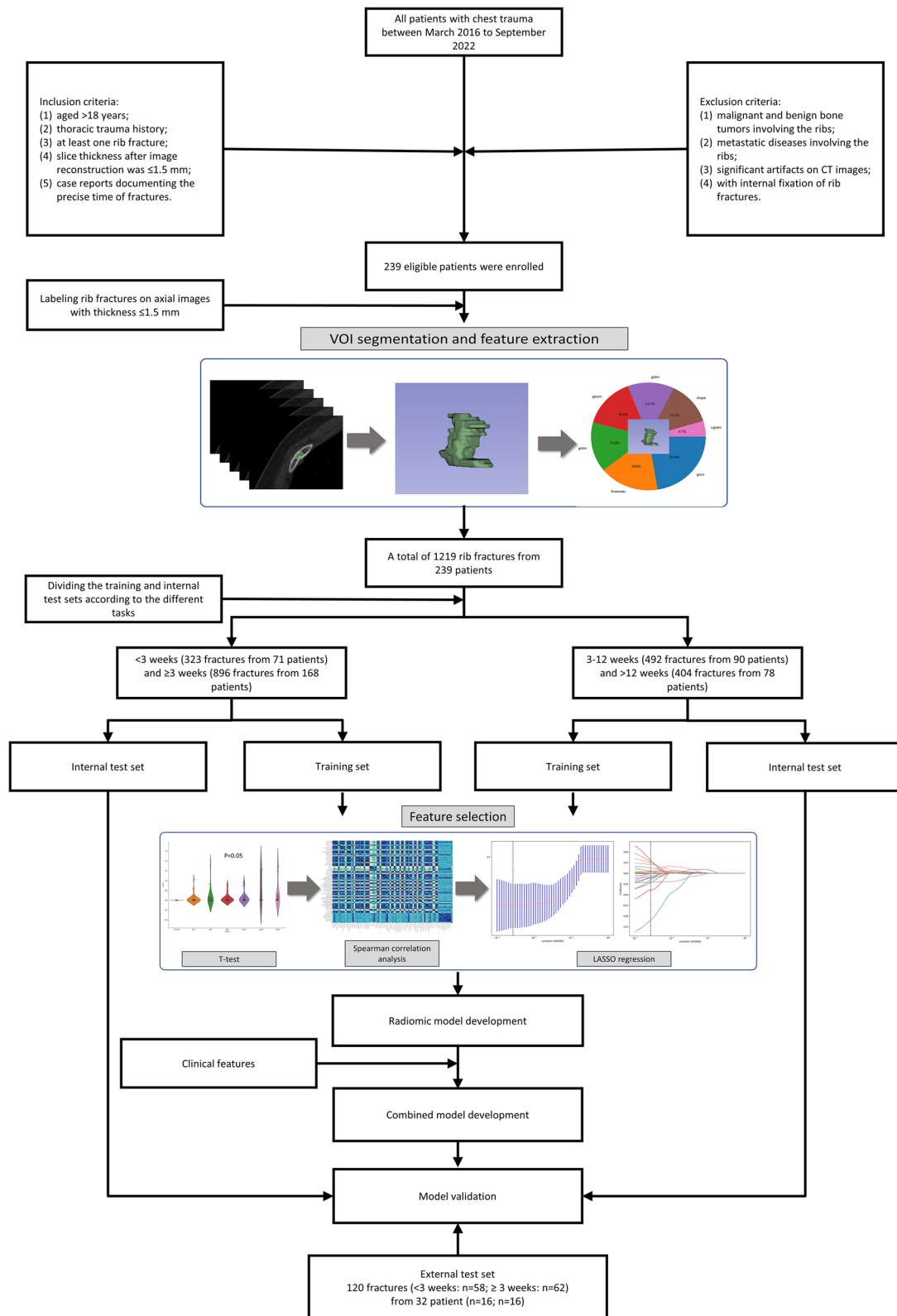
Fig. 1 Flow chart of the recruitment pathway for the datasets used in this study

Tang *et al. Insights into Imaging* (2023) 14:214

Page 5 of 13

algorithms, support vector machine (SVM), K-nearest neighbor, random forest, decision tree, and eXtreme Gradient Boosting to determine the most suitable classifier for fracture age assessment. Hyperparameters were optimized using grid search and tenfold cross-validation. Only the hyperparameters listed in Table S4 were adjusted, while all other hyperparameters were maintained at the default values specified by models. The filtered radiomic features were incorporated into the classifier and trained within the training set to obtain the radiomic model.

Using one of the two levels of binary classification (< 3 weeks or 3–12 weeks) as the reference standard, coded as 0 in the training of the classifier, we obtained the predicted probability of each fracture in the remaining two groups as the radiomic signature. Lastly, we developed the combined model based on the radiomic signature and clinical features using multivariate logistic regression.

Nomogram building

In order to simplify the combined model into an easy-to-understand tool, a nomogram was utilized for constructing a simplified graphical display. The sum of nomogram points was calculated based on clinical features and radiomic signature. For the convenience of calculations, instantly deployable online calculators were developed.

Statistical analysis

Statistical analysis was performed using SPSS 26.0 (IBM) and R Studio (ver. 4.3.1). Clinical features were measured using chi-squared or Fisher's exact-probability testing as all were categorical variables. The clinical features with p values of < 0.05 in both univariate and multivariate logistic regression analyses were included in the combined model. Differences in radiomic features were assessed using the t-test or the Mann–Whitney U test as they were continuous variables. The statistical significance level was set at p values of < 0.05.

Results

Selection of clinical features

The clinical features were compared (Table S1 and S2), and we observed no significant differences between the clinical features of the training and internal test sets ($p = 0.142$–0.988). Results of univariate and multivariate logistic regression analyses for clinical features associated with the classification of fracture age are presented in Table 1. For classifying fracture age between < 3 and ≥ 3 weeks, six independent clinical features were selected, including sex, fractures of ribs 1–4, pleural inflammation, lateral fractures,

intramedullary callus formation, and periosteal callus formation. For classifying fracture age between 3–12 and > 12 weeks, three independent clinical features were selected, including pleural inflammation, intramedullary callus formation, and multiple fractures of the same rib.

Table 1 Results of univariate and multivariate logistic regression analyses for classification of fracture age

	Standard error	Odds ratio	p value
Classification of fracture age (< 3 weeks vs ≥ 3 weeks)			
Results of univariate analysis			
Age	0.007	1.012	0.117
Sex	0.170	0.667	0.017
Ribs 1–4 fractures	0.077	2.630	< 0.001
Pleural inflammation	0.209	0.257	< 0.001
Lateral fractures	0.198	2.267	< 0.001
Bone fragments	0.372	0.512	0.072
Multiple fractures of the same rib	0.160	1.582	0.004
Cartilage junction fractures	0.077	2.630	< 0.001
Periosteal callus information	0.077	2.630	< 0.001
Intramedullary callus information	0.180	6.706	< 0.001
Positive results of multivariate logistic regression analysis			
Sex	0.234	2.189	0.001
Ribs 1–4 fractures	0.199	2.060	< 0.001
Pleural inflammation	0.254	0.238	< 0.001
Lateral fractures	0.238	2.189	0.001
Periosteal callus formation	0.222	5.236	< 0.001
Intramedullary callus formation	3.565	3.565	< 0.001
Classification of fracture age (3–12 weeks vs > 12 weeks)			
Results of univariate analysis			
Age	0.009	1.010	0.274
Sex	0.168	0.595	0.020
Ribs 1–4 fractures	0.165	1.401	0.041
Pleural inflammation	0.399	0.246	< 0.001
Lateral fractures	0.172	1.273	0.161
Bone fragments	0.523	0.402	0.082
Multiple fractures of the same rib	0.165	0.492	< 0.001
Cartilage junction fractures	0.250	1.025	0.920
Periosteal callus formation	0.167	0.592	0.002
Intramedullary callus information	0.270	0.258	< 0.001
Positive results of multivariate logistic regression analysis			
Pleural inflammation	0.419	0.244	0.001
Multiple fractures of the same rib	0.175	0.528	< 0.001
Intramedullary callus formation	0.305	0.334	< 0.001

Tang *et al. Insights into Imaging*   (2023) 14:214

Page 6 of 13

Development and validation of the radiomic model

Using the < 3 weeks as the reference standard, 17 radiomic features were obtained using the *t*-test, Spearman's correlation analysis, and LASSO regression analysis, including 3 shape, 4 intensity, and 10 texture features (Figure S2).

Using the 3–12 weeks as the reference standard, 10 radiomic features were obtained using the *t*-test, Spearman's correlation analysis, and LASSO regression analysis, including 3 shape, 2 intensity, and 5 texture features (Figure S3).

SVM performed the best on fracture age assessment (Table S5); therefore, we chose it as the base classifier for the radiomic model and obtained the radiomic signature. Regarding the classification of the fracture age between < 3 weeks and ≥ 3 weeks, using < 3 weeks as the reference standard, the performance of the radiomic model showed an AUC of 0.897 (95% confidence interval [CI]: 0.875–0.925) and 0.854 (95% CI: 0.804–0.903) for the training and internal test sets, respectively. Regarding the classification of the fracture age between 3–12 weeks and > 12 weeks, using 3–12 weeks as the reference standard, the performance of the radiomic model showed an AUC of 0.837 (95% CI: 0.805–0.868) and 0.793 (95% CI: 0.738–0.847) for the training and internal test sets, respectively.

Development and visualization of the combined model

For classifying fracture age between < 3 and ≥ 3 weeks, using the selected clinical features and radiomic signature, a combined model was developed and visualized in the form of a nomogram (Fig. 2). The online version of the nomogram could be used at https://myr234r. shinyapps.io/DynNomapp3/, and its user interface is illustrated in Fig. 4a. The AUC values of the combined model were 0.914 (95% CI = 0.892–0.935) and 0.889 (95% CI = 0.846–0.932) for the training and internal test sets, respectively. The calibration curves revealed good predictive accuracy between the actual probability and predicted probability (Fig. 2).

For classifying fracture age between 3–12 and > 12 weeks, using the selected clinical features and radiomic signature, a combined model was developed and visualized in the form of a nomogram (Fig. 3). An online version of the nomogram could be used at https://myr234r.shinyapps.io/DynNomapp12/ and its user interface is illustrated in Fig. 4b. The AUC values of the combined model were 0.848 (95% CI: 0.818–0.878) and 0.818 (95% CI: 0.767–0.869) in the training and internal test sets, respectively. The calibration curves of the nomogram showed acceptable agreement between prediction and actual observation (Figs. 2 and 3).

Performance comparison between the radiomic and combined models

The DeLong test showed that the combined model performed better than the radiomic model for classification between < 3 weeks, ≥ 3 weeks, 3–12 weeks, and > 12 weeks (Table 2).

For classifying fracture age between < 3 weeks and ≥ 3 weeks, the receiver operating characteristic (ROC) curves of the radiomic and combined models are shown in Fig. 5. In the training set, the combined model (AUC = 0.915, 95% CI = 0.893–0.936) outperformed the radiomic model (AUC = 0.900, 95% CI = 0.875–0.925; *p* = 0.009). Similarly, in the internal test set, the combined model (AUC = 0.889, 95% CI = 0.846–0.932) outperformed the radiomic model (AUC = 0.854, 95% CI = 0.804–0.903; *p* < 0.001).

For classifying the fracture age between 3–12 weeks and > 12 weeks, the ROC curves of the radiomic and combined models are shown in Fig. 5. In the training set, the AUC of the combined model (0.848, 95% CI = 0.818–0.878) was slightly higher than that of the radiomic model (0.837, 95% CI = 0.805–0.868; *p* = 0.12). However, in the internal test set, the combined model (AUC = 0.818, 95% CI = 0.767–0.869) performed significantly better than the radiomic model (AUC = 0.793, 95% CI = 0.738–0.847; *p* = 0.003).

Performance in the external test set

In the external test set, we reached the same conclusion as that in the internal dataset (Table 3). We evaluated a radiologist's (engaged in musculoskeletal imaging diagnosis for 15 years) performance in classifying rib fracture age aided by the combined model. For classifying fracture age between < 3 and ≥ 3 weeks, the AUC values for the radiomic model, combined model, and radiologist aided by the combined model were 0.811 (95% CI = 0.733–0.889), 0.881 (95% CI = 0.814–0.949), and 0.966 (95% CI = 0.935–0.996), respectively. This indicated that the combined model was better than the radiomic model, and the collaborative integration of the radiologist with the combined model further enhanced classification performance (Figure S4).

Discussion

The results from the current study showed that our combined model, based on clinical and radiomic features, could accurately classify the age of rib fractures. The good performance of the radiologist assisted by the model demonstrated the potential feasibility of the model in practical applications, and it is expected to provide value for clinical and forensic decision-making.

Tang *et al. Insights into Imaging*   (2023) 14:214

Page 7 of 13
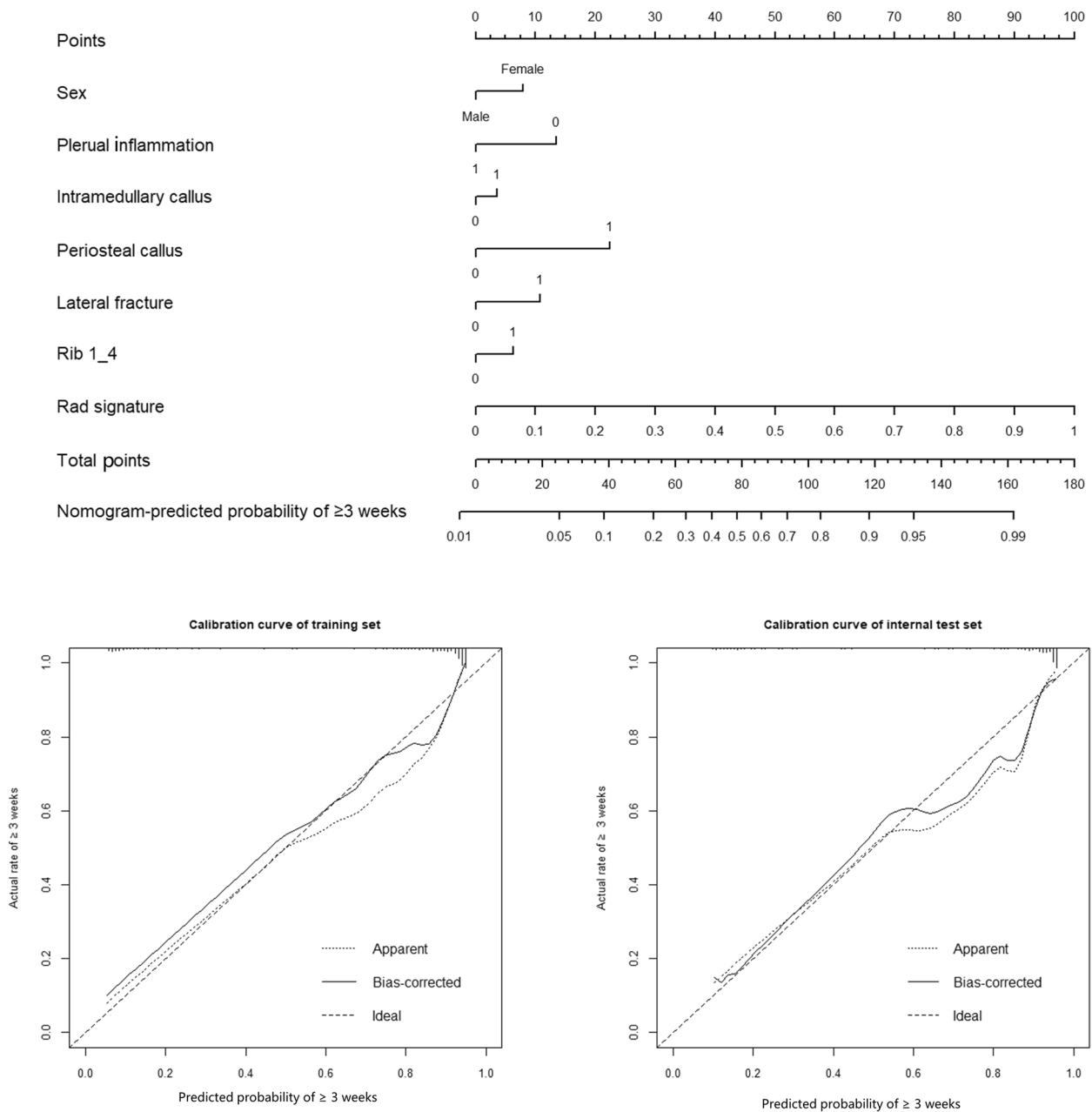
Fig. 2 The combined model for classification between < 3 weeks and ≥ 3 weeks. The calibration curves of this model in the training and internal test sets were obtained by resampling 1000 times. The dotted line indicates the ideal ability, and the solid line represents the real ability of the model. The combined performed better when the solid line was closer to the dotted line

After a fracture, the fracture region undergoes a series of characteristic events over time called the inflammatory, repair, and remodeling phases, all of which are influenced by many complex factors [21, 22]. Sex, 1–4 rib fractures, and lateral fractures impact fracture healing through estrogen levels, vascular injury, and respiration and body movements, respectively [14, 23–26]. Pleural inflammation and callus formation are considered important imaging features of the inflammatory and reparative phases of fracture healing, respectively [21, 27]. In late fracture healing, multiple fractures of the same rib end healing early by promoting bone resorption [28]. Therefore, the above clinical features were included in our combined model. Radiomic enables the quantification of heterogeneity of fracture regions, thereby compensating for the limitations of visual image assessment.

Tang *et al. Insights into Imaging* (2023) 14:214

Page 8 of 13
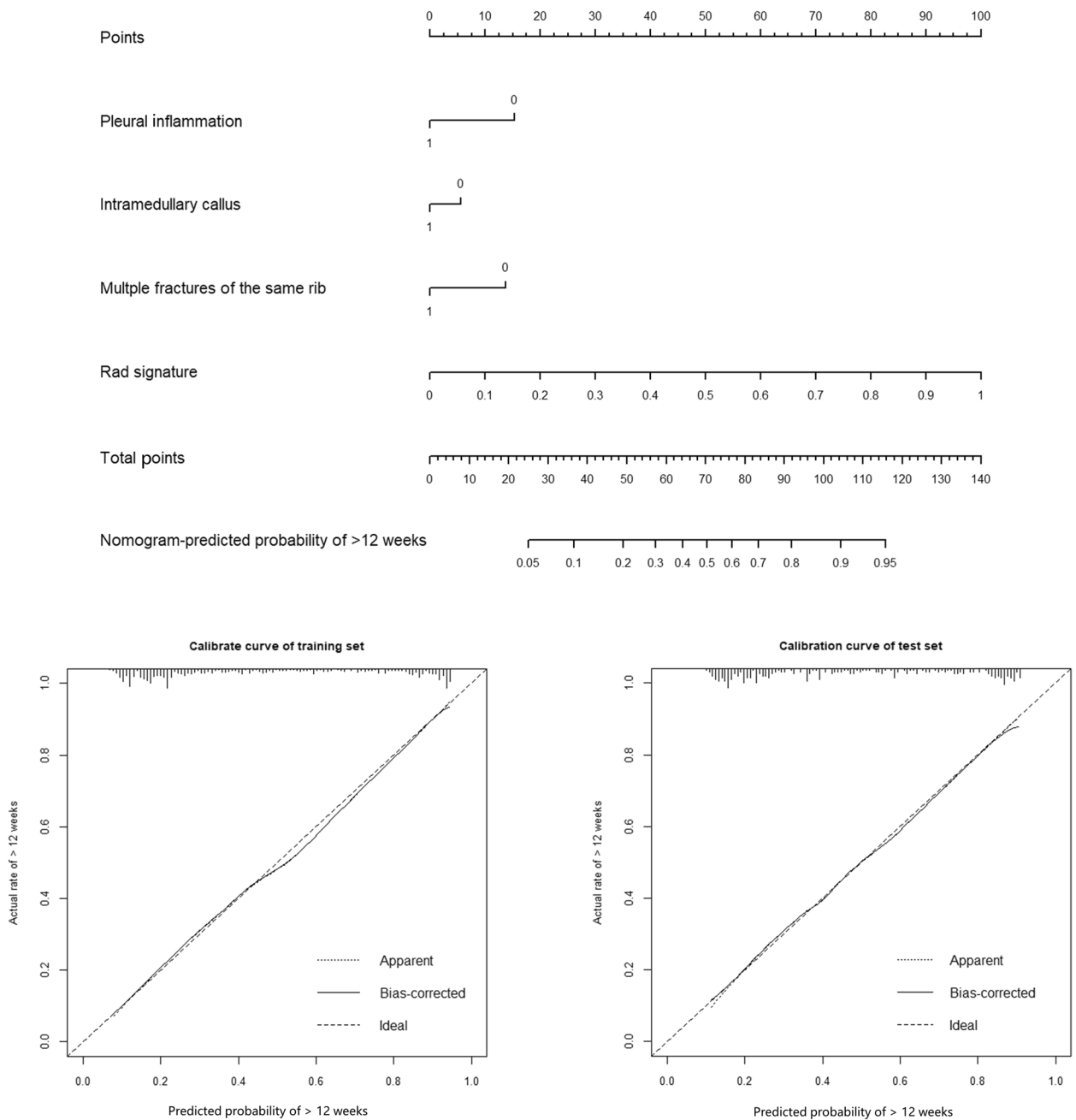
Fig. 3 The combined model for classification between 3–12 weeks and > 12 weeks. The calibration curves of this model in the training and internal test sets were obtained by resampling 1000 times. The dotted line indicates the ideal ability, and the solid line represents the real ability of the model. The combined performed better when the solid line was closer to the dotted line

The combination of all pertinent features (visually observable clinical features and visually difficult-to-identify radiomic features) in the combined model allows for a comprehensive assessment of fracture regions, providing radiologists with additional data-driven insights. Thus, aided by the combined model, radiologists achieve diagnoses by integrating subjective and objective interpretations of medical images, together with their individual clinical experience. This fusion of knowledge from both human expertise and data-driven analysis enhances the diagnostic decision-making process, ultimately improving diagnostic performance.
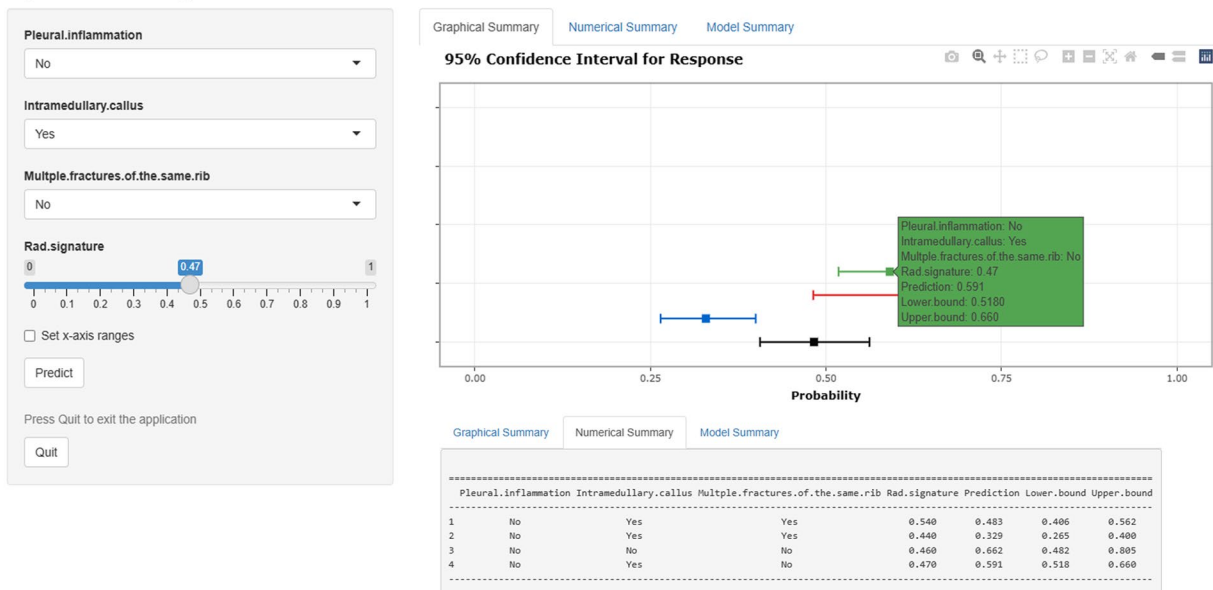
Fig. 4 Online dynamic nomograms for classifying rib fracture age between < 3 and ≥ 3 weeks (**a**) and between 3–12 weeks and > 12 weeks (**b**). The figure displays the probabilities (with a 95% confidence interval) determined by the combined model for rib fracture ages of ≥ 3 weeks and > 12 weeks. The specific predicted values are provided in the "Numerical Summary" tab

Radiomics are useful for detecting changes in bone microarchitecture due to injury and aging [29–32]. Several studies [33–35] utilized radiomic features from T2-weighted images to achieve early diagnosis of osteoarthritis. Lin et al. [36] developed a radiomic and clinical features-based model to predict the prognosis of osteoarthritis, with an AUC of 0.83 (95% CI = 0.70–0.96) in the validation set. Recent studies [37–45] also

demonstrated the ability of radiomics in osteoporosis detection and fracture prediction. Apart from its applications in diagnosing bone disorders, radiomics research is starting to emerge in the field of forensic medicine. Giorgio et al. [46] demonstrated, based on a limited sample ($n = 4$), that CT-based radiomics could be associated with time of death. Subsequently, Klontzas et al. [47] applied CT-based radiomics to predict

Tang *et al. Insights into Imaging* (2023) 14:214

Page 10 of 13

Table 2 Performance comparison of the radiomic and combined models

Model		AUC	*p* value	SENS	SPEC
< 3 weeks vs ≥ 3 weeks					
Radiomic model	T	0.900 (0.875–0.925)	Reference	0.857 (0.763–0.908)	0.855 (0.763–0.919)
	I-T	0.854 (0.804–0.903)		0.812 (0.74–0.924)	0.798 (0.663–0.876)
Combined model	T	0.915 (0.894–0.937)	0.009	0.851 (0.759–0.923)	0.838 (0.744–0.923)
	I-T	0.897 (0.857–0.938)	< 0.001	0.820 (0.729–0.903)	0.888 (0.775–0.995)
3–12 weeks vs > 12 weeks					
Radiomic model	T	0.837 (0.805–0.868)	Reference	0.729 (0.593–0.825)	0.855 (0.763–0.919)
	I-T	0.793 (0.738–0.847)		0.816 (0.740–0.931)	0.798 (0.663–0.876)
Combined model	T	0.848 (0.818–0.878)	0.12	0.732 (0.650–0.800)	0.836 (0.775–0.899)
	I-T	0.818 (0.767–0.869)	0.003	0.718 (0.597– 0.879)	0.821 (0.628–0.910)

AUC area under the receiver operating characteristic curve, *SENS* sensitivity, *SPEC* specificity, *T* training set, *I-T* internal test set
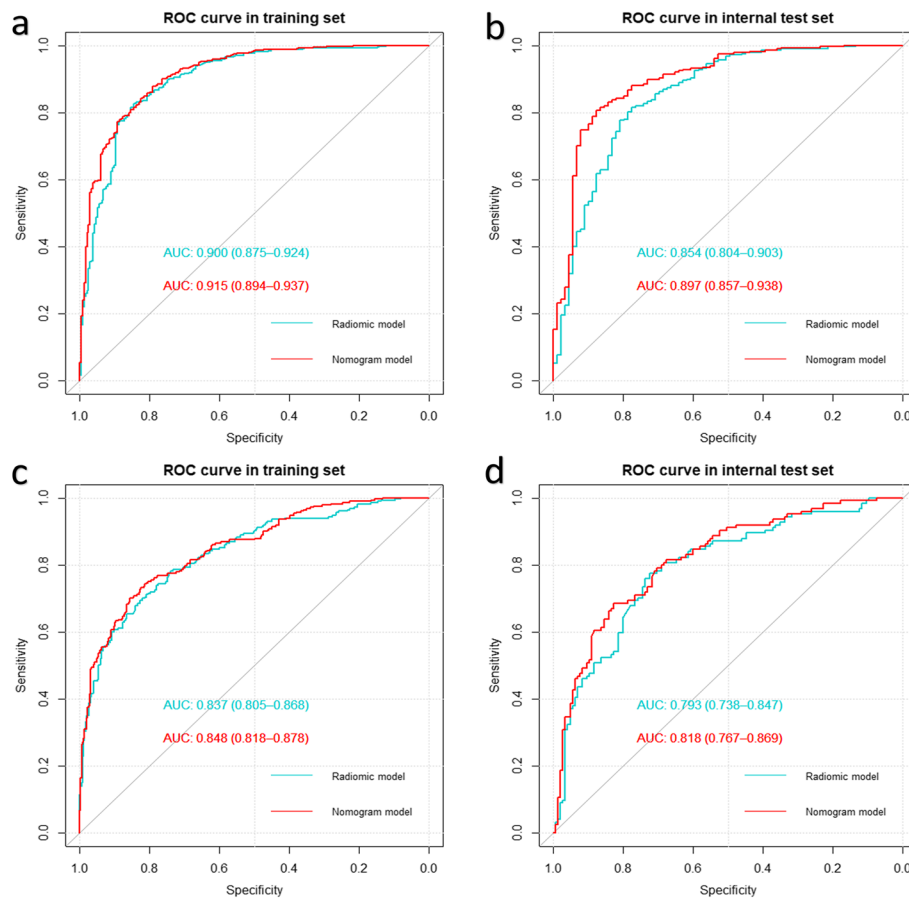
Fig. 5 Receiver operating characteristic (ROC) analysis revealed that for the classification between < 3 and ≥ 3 weeks (**a**, **b**), as well as between 3–12 and > 12 weeks (**c**, **d**), the performance of the combined model (red line) surpassed that of the radiomics model (blue line) in both the training and internal test sets

postmortem interval, yielding promising results in this exploratory study (AUC = 0.75, 95%CI = 0.584–0.916). A previous forensic study [48] indicated an association between CT-based quantitative parameters and the age of rib fractures. However, the limited sample size ($n = 9$) and the finite number of extracted features ($n = 5$)

were insufficient for conducting ML analysis. The aforementioned radiomics research in forensic medicine predominantly focused on postmortem forensic investigations, whereas this study pertained to trauma assessment for legal proceedings. Our study was based on principles similar to those of the aforementioned

Table 3 Performance comparison of the radiomic model, combined model, and nomogram-assisted radiologist for classifying fracture age between < 3 and ≥ 3 weeks in the external test set

Model	AUC	*p* value	SENS	SPEC
Radiomic model	0.811 (0.733–0.889)	0.003	0.871 (0.548–0.968)	0.690 (0.535–0.966)
Combined model	0.881 (0.814–0.949)	Reference	0.887 (0.742–0.968)	0.862(0.724–0.966)
Radiologist aided by the combined model	0.966 (0. 935–0.996)	0.007	0.984 (0.887–1)	0.897 (0.793–0.966)

AUC area under the receiver operating characteristic curve, *SENS* sensitivity, *SPEC* specificity

studies, namely, that radiomics, which reflect changes in bone microstructure during the bone healing process, can be used for fracture age classification, and that the addition of clinical features can further enhance model performance.

A strength of this study is the development of a single radiomic signature that summarizes various radiomic features, providing a useful tool for clinical practice. In addition, the combined model was visualized as a nomogram, providing readers with more tangible interpretation of each factor's impact on the classification. We have made our combined model public on an open-access website in the form of online calculator to simplify the calculations. However, some limitations exist in our study. First, this was a retrospective study. A prospective study is needed to further validate our model. Second, older participants were included in this study (median age, 57 years; interquartile range, 50–63 years) and the model's applicability to younger patients is unknown. Younger patients should be included in future studies to improve the robustness of the model. Lastly, in the absence of data > 12 weeks from the external center, we did not perform external validation for the model in classifying fracture age between 3–12 and > 12 weeks. Future studies could be designed to overcome these limitations.

Conclusions

Our study established a combined model for rib fracture age classification based on CT images. The combined model and the model-assisted radiologist achieved good performance in classifying rib fracture age. This model has the potential to influence clinical practice and forensic decision-making.

Abbreviations

AUC	Area under the curve
CI	Confidence interval
LASSO	Least absolute shrinkage and selection operator
OR	Odds ratio
ROC	Receiver operating characteristic
SVM	Support vector machine
VOI	Volume of interest

Supplementary Information

The online version contains supplementary material available at https://doi.org/10.1186/s13244-023-01546-y.

Additional file 1: Supplementary methods. Table S1. Baseline characteristics of the internal dataset for classification between <3 and ≥3 weeks. **Table S2.** Baseline characteristics of the internal dataset for classification between 3–12 weeks and >12 weeks. **Table S3.** Baseline characteristics of the external dataset. **Table S4.** Optimal hyperparameter configuration list for machine learning algorithms. **Table S5.** Performance comparison of different models. **Figure S1.** Delineation of the volume of interest (VOI) for the rib fracture region. **Figure S2.** LASSO regression analysis procedure for the selection of radiomic features. **Figure S3.** LASSO regression analysis procedure for the selection of radiomic features. **Figure S4.** Receiver operating characteristic (ROC) comparison among radiomic model, combined model, and nomogram-assisted radiologist using the external test set.

Authors' contributions

Conceptualization, Y.T., L.J., and M.L.; methodology, Y.T., L.J., W.J., and D.L.; software, Y.T.; formal analysis, Y.T., Z.M., and L.J.; investigation, L.J.; resources, L.J. and M.L.; data curation, L.J., Y.T., W.H., and D.L.; writing—original draft, L.J.; writing—review and editing, L.J. and M.L.; supervision, W.H. and M.L.

Funding

Availability of data and materials

All the data will be shared upon reasonable request by the corresponding author.

Declarations

Ethics approval and consent to participate

This retrospective study was approved by the ethics committee of Huadong Hospital affiliated to Fudan University (NO. 20220069), which waived the requirement for informed consent.

Consent for publication

Not applicable.

Competing interests

The authors declare that they have no competing interests.

Tang *et al. Insights into Imaging*   (2023) 14:214

Page 12 of 13

Author details

[1]Radiology Department, Huadong Hospital Affiliated to Fudan University, No. 221 West Yan'an Road, Jing'an District, Shanghai 200040, China. [2]Radiology Department, Huashan Hospital Affiliated to Fudan University, Shanghai, China. [3]Radiology Department, Shanghai Electric Power Hospital, Shanghai, China. [4]Department of Geriatrics and Gerontology, Huadong Hospital Affiliated to Fudan University, No. 221 West Yan'an Road, Jing'an District, Shanghai 200040, China. [5]Institute of Functional and Molecular Medical Imaging, No. 221 West Yan'an Road, Jing'an District, Shanghai 200040, China.

References

1. Head W, Kumar N, Thomas C, Leon S, Dieffenbaugher S, Eriksson E (2021) Are rib fractures stable? An analysis of progressive rib fracture offset in the acute trauma setting. J Trauma Acute Care Surg 91:917–922
2. O'Donovan S, van den Heuvel C, Baldock M, Humphries MA, Byard RW (2022) Fatal blunt chest trauma: an evaluation of rib fracture patterns and age. Int J Legal Med 136:1351–1357
3. Yu L, Baumann BM, Raja AS et al (2020) Blunt traumatic aortic injury in the pan-scan era. Acad Emerg Med 27:291–296
4. Lafferty PM, Anavian J, Will RE, Cole PA (2011) Operative treatment of chest wall injuries: indications, technique, and outcomes. J Bone Joint Surg Am 93:97–110
5. Pieracci FM, Majercik S, Ali-Osman F et al (2017) Consensus statement: surgical stabilization of rib fractures rib fracture colloquium clinical practice guidelines. Injury 48:307–321
6. Ensrud KE (2013) Epidemiology of fracture risk with advancing age. J Gerontol A Biol Sci Med Sci 68:1236–1242
7. Bonicelli A, Kranioti EF, Xhemali B, Arnold E, Zioupos P (2022) Assessing bone maturity: compositional and mechanical properties of rib cortical bone at different ages. Bone 155:116265
8. He Z, Zhang D, Xiao H et al (2019) The ideal methods for the management of rib fractures. J Thorac Dis 11:S1078–s1089
9. Coary R, Skerritt C, Carey A, Rudd S, Shipway D (2020) New horizons in rib fracture management in the older adult. Age Ageing 49:161–167
10. Chua MT, Pan DST, Lee MZ et al (2022) Epidemiology and outcomes of older trauma patients in Singapore: a multicentre study. Injury 53:3149–3155
11. Lau G, Gabbe BJ, Giummarra MJ (2021) Patterns and predictors of personal responsibility attributions after major trauma. Injury 52:2886–2895
12. Morshed S (2014) Current options for determining fracture union. Adv Med 2014:708574
13. Zura R, Xu ZJ, Della Rocca GJ, Mehta S, Steen RG (2017) When is a fracture not "fresh"? Aligning reimbursement with patient outcome after treatment with low-intensity pulsed ultrasound. J Orthop Trauma 31:248–251
14. Fisher JS, Kazam JJ, Fufa D, Bartolotta RJ (2019) Radiologic evaluation of fracture healing. Skeletal Radiol 48:349–361
15. Gillies RJ, Kinahan PE, Hricak H (2016) Radiomics: images are more than pictures, they are data. Radiology 278:563–577
16. Abbasian Ardakani A, Bureau NJ, Ciaccio EJ, Acharya UR (2022) Interpretation of radiomics features-a pictorial review. Comput Methods Programs Biomed 215:106609
17. Wu X, Jiang Y (2015) Old fracture. Zhonghua Wai Ke Za Zhi 53:460–463
18. Arredondo-Gómez E (2007) Treatment of traumatic clavicular pseudoarthrosis with the Hunec Colchero nail. Acta Ortop Mex 21:63–68
19. van Griethuysen JJM, Fedorov A, Parmar C et al (2017) Computational radiomics system to decode the radiographic phenotype. Cancer Res 77:e104–e107
20. Deist TM, Dankers F, Valdes G et al (2018) Machine learning algorithms for outcome prediction in (chemo)radiotherapy: an empirical comparison of classifiers. Med Phys 45:3449–3459
21. Claes L, Recknagel S, Ignatius A (2012) Fracture healing under healthy and inflammatory conditions. Nat Rev Rheumatol 8:133–143
22. Palanisamy P, Alam M, Li S, Chow SKH, Zheng YP (2022) Low-intensity pulsed ultrasound stimulation for bone fractures healing: a review. J Ultrasound Med 41:547–563
23. Talbot BS, Gange CP Jr, Chaturvedi A, Klionsky N, Hobbs SK, Chaturvedi A (2017) Traumatic rib injury: patterns, imaging pitfalls, complications, and treatment. Radiographics 37:628–651
24. Claes L (2011) Biomechanical principles and mechanobiologic aspects of flexible and locked plating. J Orthop Trauma 25(Suppl 1):S4–7
25. Rizzoli R, Reginster JY, Boonen S et al (2011) Adverse reactions and drug-drug interactions in the management of women with postmenopausal osteoporosis. Calcif Tissue Int 89:91–104
26. Fischer V, Haffner-Luntzer M (2022) Interaction between bone and immune cells: implications for postmenopausal osteoporosis. Semin Cell Dev Biol 123:14–21
27. Kolar P, Schmidt-Bleek K, Schell H et al (2010) The early fracture hematoma and its potential role in fracture healing. Tissue Eng Part B Rev 16:427–434
28. Loi F, Córdova LA, Pajarinen J, Lin TH, Yao Z, Goodman SB (2016) Inflammation, fracture and bone repair. Bone 86:119–130
29. Le Corroller T, Halgrin J, Pithioux M, Guenoun D, Chabrand P, Champsaur P (2012) Combination of texture analysis and bone mineral density improves the prediction of fracture load in human femurs. Osteoporos Int 23:163–169
30. Xuan A, Chen H, Chen T et al (2023) The application of machine learning in early diagnosis of osteoarthritis: a narrative review. Ther Adv Musculoskelet Dis 15:1759720x231158198
31. Fritz B, Yi PH, Kijowski R, Fritz J (2023) Radiomics and deep learning for disease detection in musculoskeletal radiology: an overview of novel MRI- and CT-based approaches. Invest Radiol 58:3–13
32. Levi R, Garoli F, Battaglia M et al (2023) CT-based radiomics can identify physiological modifications of bone structure related to subjects' age and sex. Radiol Med 128:744–754
33. Peuna A, Hekkala J, Haapea M et al (2018) Variable angle gray level co-occurrence matrix analysis of T(2) relaxation time maps reveals degenerative changes of cartilage in knee osteoarthritis: Oulu knee osteoarthritis study. J Magn Reson Imaging 47:1316–1327
34. Xie Y, Dan Y, Tao H et al (2021) Radiomics feature analysis of cartilage and subchondral bone in differentiating knees predisposed to posttraumatic osteoarthritis after anterior cruciate ligament reconstruction from healthy knees. Biomed Res Int 2021:4351499
35. Hirvasniemi J, Klein S, Bierma-Zeinstra S, Vernooij MW, Schiphof D, Oei EHG (2021) A machine learning approach to distinguish between knees without and with osteoarthritis using MRI-based radiomic features from tibial bone. Eur Radiol 31:8513–8521
36. Lin T, Peng S, Lu S et al (2023) Prediction of knee pain improvement over two years for knee osteoarthritis using a dynamic nomogram based on MRI-derived radiomics: a proof-of-concept study. Osteoarthritis Cartilage 31:267–278
37. Farzi M, Pozo JM, McCloskey E et al (2022) Quantitating age-related BMD textural variation from DXA region-free-analysis: a study of hip fracture prediction in three cohorts. J Bone Miner Res 37:1679–1688
38. Hong N, Park H, Kim CO et al (2021) Bone radiomics score derived from DXA hip images enhances hip fracture prediction in older women. J Bone Miner Res 36:1708–1716
39. Rastegar S, Vaziri M, Qasempour Y et al (2020) Radiomics for classification of bone mineral loss: a machine learning study. Diagn Interv Imaging 101:599–610
40. Huang CB, Hu JS, Tan K, Zhang W, Xu TH, Yang L (2022) Application of machine learning model to predict osteoporosis based on abdominal computed tomography images of the psoas muscle: a retrospective study. BMC Geriatr 22:796
41. Dai H, Wang Y, Fu R et al (2023) Radiomics and stacking regression model for measuring bone mineral density using abdominal computed tomography. Acta Radiol 64:228–236
42. Zhang J, Liu J, Liang Z et al (2023) Differentiation of acute and chronic vertebral compression fractures using conventional CT based on deep transfer learning features and hand-crafted radiomics features. BMC Musculoskelet Disord 24:165
43. Biamonte E, Levi R, Carrone F et al (2022) Artificial intelligence-based radiomics on computed tomography of lumbar spine in subjects with fragility vertebral fractures. J Endocrinol Invest 45:2007–2017
44. Zhang H, Yuan G, Wang C et al (2023) Differentiation of benign versus malignant indistinguishable vertebral compression fractures by

different machine learning with MRI-based radiomic features. Eur Radiol 33:5069–5076

45. Chen YC, Li YT, Kuo PC et al (2023) Automatic segmentation and radiomic texture analysis for osteoporosis screening using chest low-dose computed tomography. Eur Radiol 33:5097–5106

46. De-Giorgio F, Ciasca G, Fecondo G et al (2022) Post mortem computed tomography meets radiomics: a case series on fractal analysis of post mortem changes in the brain. Int J Legal Med 136:719–727

47. Klontzas ME, Leventis D, Spanakis K, Karantanas AH, Kranioti EF (2023) Post-mortem CT radiomics for the prediction of time since death. Eur Radiol 33(11):8387–8395.

48. Viero A, Biehler-Gomez L, Messina C et al (2022) Utility of micro-CT for dating post-cranial fractures of known post-traumatic ages through 3D measurements of the trabecular inner morphology. Sci Rep 12:10543

Publisher's Note

Springer Nature remains neutral with regard to jurisdictional claims in published maps and institutional affiliations.